Inhibition of the membrane repair protein annexin-A2 prevents tumour invasion and metastasis

Céline Gounou, Flora Bouvet, Léna d'Agata, Marie-Alix Derieppe, Lucile Rouyer, Léa Bouton, Mailys Mélane, Dorian Chapeau, Etienne Harté, Julie Martineau, et al.

Inhibition of the membrane repair protein annexin-A2 prevents tumour invasion and metastasis

Céline Gounou
CNRS, University of Bordeaux, IPB
Flora Bouvet
Léna d'Agata
CNRS, University of Bordeaux, IPB
Marie-Alix Derieppe
Inserm
Lucile Rouyer
Univ. Bordeaux, INSERM - BRIC, U 1312
Léa Bouton
Univ. Bordeaux, INSERM - BRIC, U 1312
Mailys Mélane
Univ. Bordeaux, CNRS, LOMA, UMR 5798
Dorian Chapeau
Univ. Bordeaux, CNRS, Bordeaux INP, CBMN, UMR 5248
Etienne Harté
Univ. Bordeaux, CNRS, LOMA, UMR 5798
Julie Martineau
Univ. Bordeaux, Animalerie Mutualisée, Service Commun des Animaleries
Valerie Prouzet-Mauleon
University of Bordeaux
Sisareuth Tan
University of Bordeaux
Wilfried Souleyreau
Univ. Bordeaux, INSERM, BRIC, U 1312
Frederic Saltel
University of Bordeaux, Inserm, UMR1312, BRIC, BoRdeaux Institute of onColoy-Oncoprot, UAR 005 TBMcore- University of Bordeaux, Plateforme Protéome
Francoise Argoul
Laboratoire Ondes et Matière d'Aquitaine
Geraldine Siegfried
INSERM
Abdel-Majid Khatib

Angiogenesis and Cancer Microenvironment Laboratory

Alain Brisson

University of Bordeaux

Richard Iggo

Univ. Bordeaux, INSERM, BRIC, U 1312

Anthony Bouter (anthony.bouter@u-bordeaux.fr)

CNRS, University of Bordeaux, IPB

Article

Keywords: Cancer, metastasis, invasion, membrane repair, ANXA2, annexin-A2, annexins

Posted Date: November 9th, 2022

DOI: https://doi.org/10.21203/rs.3.rs-2252278/v1

Inhibition of the membrane repair protein annexin-A2 prevents tumour invasion and metastasis

Gounou C.[1], Bouvet F.[1], d'Agata L.[1], Derieppe M.A.[2], Rouyer L.[3], Bouton L.[3], Mélane M.[4], Chapeau D.[1], Harté E.[4], Martineau J.[2], Prouzet-Mauleon V.[3,5], Tan S.[1], Souleyreau W.[3], Saltel F.[3], Argoul F.[4], Siegfried G.[3,6], Khatib M.[3,6,7], Brisson A.R.[1], Iggo R.[3], Bouter A.[1,*]

[1] Univ. Bordeaux, CNRS, Bordeaux INP, CBMN, UMR 5248, F-33600 Pessac, France
[2] Univ. Bordeaux, Animalerie Mutualisée, Service Commun des Animaleries, F-33000 Bordeaux, France.
[3] Univ. Bordeaux, INSERM, BRIC, U 1312, F-33000 Bordeaux, France
[4] Univ. Bordeaux, CNRS, LOMA, UMR 5798, F-33400 Talence, France
[5] CRISPRedit, TBMcore, UAR CNRS 3427, Inserm US 005, Univ. Bordeaux,
[6] XenoFish, B2 Ouest, Allée Geoffroy St Hilaire CS50023, Pessac 33615, France
[7] Bergonié Institute, Bordeaux, France.

*Corresponding author
Mailing address: Bât. B14, Allée Geoffroy Saint Hilaire, 33600 Pessac, France
E-mail: a.bouter@cbmn.u-bordeaux.fr; Tel: +33 540006860 ; Fax : +33 540002200

Abstract

Cancer cells are exposed to major compressive and shearing forces during invasion and metastasis, leading to extensive plasma membrane damage. To survive this mechanical stress, they need to repair membrane injury efficiently. Targeting the membrane repair machinery is thus potentially a new way to prevent invasion and metastasis. We show here that annexin-A2 (ANXA2) is required for membrane repair in MDA-MB-231 cells, a highly invasive triple-negative breast cancer cell line. Mechanistically, we show by fluorescence and electron microscopy that cells fail to reseal membrane damaged by shear stress when ANXA2 is silenced or the protein is inhibited with neutralizing antibody. Silencing of ANXA2 has no effect on proliferation *in vitro*, and even accelerates migration in wound healing assays, but reduces tumor cell dissemination in both mice and zebrafish. We show that high expression of ANXA2 predicts poor prognosis in high-grade lung, ovarian, gastric and breast cancers. We expect that inhibiting membrane repair will be particularly effective in these aggressive, poor prognosis tumors because they rely on the membrane repair machinery to survive membrane damage during tumor invasion and metastasis. This could be achieved either with monoclonal anti-ANXA2 antibodies, which have been shown to inhibit metastasis of MDA-MB-231 cells, or with small molecule drugs.

Keywords: Cancer, metastasis, invasion, membrane repair, ANXA2, annexin-A2, annexins.

Abbreviations: ANXA1, annexin-A1; ANXA2, annexin-A2; ANXA5, annexin-A5; ANXA6, annexin-A6; Ca^{2+}, calcium; DPBS, Dulbecco's phosphate buffer saline; MOI, multiplicity of infection.

Introduction

In cells exposed to mechanical stress, plasma membrane disruption is a physiological event that occurs frequently, especially in muscle, epithelial or endothelial cells, submitted respectively to muscle contraction/stretching, and fluid or hemodynamic shear stress[1]. These cells possess a membrane repair machinery enabling to reseal injuries on a minute scale[1]. The absence of membrane repair leads to cell death and may contribute to the development of degenerative diseases such as muscular dystrophies[2]. Influx of Ca^{2+} from the extracellular (mM) to the intracellular milieu (µM) is the main trigger of membrane repair, which mainly relies on proteins that bind to membranes in a Ca^{2+}-dependent manner, such as dysferlin, AHNAK or annexins[3–5]. Twelve members, named ANXA1 to A13 (the number 12 is not assigned) compose the annexin family in mammals[6]. They are cytosolic proteins that share the property of binding to membranes exposing negatively-charged phospholipids, when Ca^{2+} concentration rises. Annexins are involved in membrane repair at different stages. ANXA1 and A2 trigger the fusion of intracellular vesicles and the recruitment to the disruption site of the new-formed lipid patch, which is responsible for membrane resealing[3]. We have shown that ANXA5 self-assembles around the disruption site in order to strengthen the membrane, preventing the expansion of the tear, and thus facilitating the repair process[4,7,8]. ANXA4 and ANXA6 are also essential for membrane repair by remodeling the damaged plasma membrane, though their specific role remains to be clarified[5,9].

Cancer metastasis results from a cascade of events that cause the disease to spread through blood or lymph, from the primary tumor to other organs. All along these processes, cancer cells are exposed to permanent mechanical stresses, which change in geometry, scale, and strength, depending on the transformation they are involved in[10]. From volume compression in the primary tumor, mechanical constraints evolve towards hemodynamic and mechanical shear stress when metastatic cells travel the bloodstream, and finally towards adhesive stretch and tight constriction, when they reach very narrow vessels and process to extravasation throughout endothelium, respectively[11,12]. These mechanical stresses are susceptible to create plasma membrane disruption in cancer cells, which account for an efficient membrane repair machinery to cope with such damages[10,13]. Although very powerful, the membrane repair machinery may be fragile and could be disturbed, constituting the Achilles' heel of cancer cells. Verifying such a hypothesis would open the way to the development of new therapeutic strategies to hamper tumor invasion and annihilate metastasis. While few studies have associated membrane repair and cancer, many publications have fortuitously reported a positive

correlation between key players of membrane repair and tumor invasion[14–16]. In addition, our experimental data provided recently a proof of principle *in cellulo*[17]. We have shown that the migration of cancer cells on fibrillar collagen induces membrane damages, whose resealing involve annexins that are highly expressed in invasive cancer cells[17]. When annexins are silenced, cancer cells migration on fibrillar collagen leads to cell death due to a defect in membrane repair[17].

The main objective of the current study was to assess if the inhibition of a key membrane repair protein in cancer cells may affect *in vivo* tumoral progression. ANXA2 was expected to provide a relevant target, since it promotes cancer progression in estrogen receptor negative breast cancers, including the aggressive triple negative sub-type[18], as well as tumoral invasion in glioblastoma[19]. In addition, ANXA2 has been reported to play a crucial role in membrane repair of human skeletal muscle cells[20–22], endothelial cells[23], and cancer cells as well[24]. We therefore generated an ANXA2 defective MDA-MB-231 cell line, for which we observed a membrane repair deficiency, as expected. We show that the inhibition of ANXA2 prevents tumor invasion and metastasis process of MDA-MB-231 cells injected in mice or zebrafish. *In vitro* analysis demonstrates that the deficiency in ANXA2 inhibits cancer cells response to shear-stress, which leads to cell death due to the absence of membrane repair. Finally, we show that a monoclonal anti-ANXA2 antibody interferes with the function of ANXA2 in membrane repair of control MDA-MB-231 cells, suggesting that it may constitute a relevant tool to inhibit tumor invasion and metastasis.

Results

ANXA2 is highly expressed in MDA-MB-231 breast cancer cells

To explore the role of annexins in breast cancer, we first compared the expression of ANXA1, ANXA2 and ANXA4 in MDA-MB-231 and MCF7 cells by Western blotting (**Figure 1 and Supplementary Figure 1**). MDA-MB-231 is a highly invasive, hormone receptor negative breast cancer cell line, whereas MCF7 is an estrogen receptor positive cell line with lower invasiveness properties[25,26]. We observed that ANXA1 and A2 were expressed at higher levels in MDA-MB-231 cells than in MCF7 cells. This result suggests that higher expression of membrane repair proteins may contribute to the more invasive phenotype of hormone receptor negative breast tumours. We chose to focus on ANXA2 in MDA-MB-231 cells in the remainder of the study because it showed the highest expression of the annexins tested, and MDA-MB-231 cells are from the highly invasive triple negative class of breast tumours.

Membrane repair in MDA-MB-231 cells requires ANXA2

Before testing the role of ANXA2 in tumor progression *in vivo*, we first examined the ability of MDA-MB-231 cells to repair membrane damage *in vitro* after silencing ANXA2 expression either by stable RNA interference, leading to a cell line hereafter named shANXA2 MDA-MB-231 (**Figure 2**), or by CRISPR-mediated deletion of ANXA2 (**Supplementary Figure 2**). We confirmed by Western blotting that ANXA2 protein expression is strongly reduced in the shANXA2 cells (**Figure 2a and Supplementary Figure 3**). Fluorescence microscopy after labelling MDA-MB-231 cells with a tdTomato-reporter revealed no significant difference in morphology after silencing ANXA2 expression (**Figure 2b**). To confirm that ANXA2 is required for membrane repair in MDA-MB-231 cells, we performed a standard membrane repair assay using laser ablation in the presence of Ca^{2+} and FM1-43[17,27]. After laser injury, FM1-43 enters the cytosol where it fluoresces upon incorporation into intracellular membranes. This fluorescence increases until the plasma membrane is resealed. In control MDA-MB-231 cells, we observed that FM1-43 entered the cell at the site of membrane irradiation within seconds of laser injury, confirming the presence of membrane rupture (**Figure 2c, +1.6 s, arrow**). After 120 s, most damaged cells exhibited an increase of intracellular fluorescence limited to the area close to the disruption site (**Figure 2c, +120 s, arrow**). The kinetics of the change in fluorescence intensity showed that intracellular fluorescence intensity increased for about 80 s and then reached a plateau (**Figure 2d, filled circles**), indicating rapid resealing of the plasma membrane. In contrast, when shANXA2 MDA-MB-231 cells were irradiated, they showed a much larger increase in fluorescence intensity (**Figure 2e and 2d),** indicating the

absence of membrane resealing. Most key membrane repair proteins are rapidly recruited to the site of membrane damage either to participate in the formation of the lipid patch by fusion of intracellular vesicles or for remodeling the damaged plasma membrane[22]. To test whether ANXA2 is recruited to the site of damage, we transfected the shANXA2 MDA-MB-231 cells with an ANXA2-GFP vector and analyzed the intracellular trafficking of ANXA2 after membrane injury by laser ablation. We observed that ANXA2-GFP was consistently recruited to the membrane disruption site in a few seconds (**Figure 2f**). To rule out a role for GFP in this process, we localized endogenous ANXA2 by immunofluorescence in laser-damaged control cells, as previously described[8,28]. This confirmed that ANXA2 is recruited to the membrane disruption site (**Figure 2g**). We conclude that ANXA2 is required for membrane repair in MDA-MB-231 cells.

Proliferation and migration *in vitro* do not require ANXA2

To investigate whether silencing of ANXA2 expression affects cell growth *in vitro*, we performed time-lapse imaging with a lens-free microscope. There was no significant difference in the growth rate of shANXA2 cells compared to control cells *in vitro*, regarding either the number of cells per time unit or the total biomass, which includes in addition the individual cell masses (**Figure 3a-b**). To test whether ANXA2 deficiency affects 2D cell migration, a wound healing assay was performed. Using a two-chamber cell-culture insert, a 500 µm-wide cell free gap was created and the ability of control or shANXA2 MDA-MB-231 cells to close the gap was assessed (**Figure 3c**). The time required for 80% wound closure was 9.8 ± 1.6 h and 6.7 ± 0.6 h for control and shANXA2 MDA-MB-231 cells, respectively (**Figure 3d**). The control and shANXA2 MDA-MB-231 cells migrated at 40.9 ± 4.1 µm/h and 67.4 ± 1.3 µm/h, respectively (**Figure 3d**). We conclude that ANXA2 deficiency slightly increases the speed of wound closure and has no effect on proliferation *in vitro*.

ANXA2 deficiency impairs membrane repair after shear stress *in vitro*

To detect differences in membrane repair after shear stress, we stained cells with DAPI after damaging the plasma membrane by repeatedly forcing the cells through a 30 Gauge needle (**Figure 4a**). To quantify differences in repair, we measured the ratio of DAPI to tdTomato fluorescence because DAPI only enters cells with damaged plasma membranes, whereas tdTomato labels all the cells. Cells are unable to repair their membranes in the absence of extracellular Ca^{2+}, so cells damaged in this condition were used as a positive control. We observed 13.6 ± 2.3 % of unrepaired cells after shear stress in the absence of Ca^{2+}, a value much

higher than in the absence of shear-stress (0.7 ± 0.5 %) (**Figure 4b, e and f**). In the presence of Ca^{2+}, the value dropped to 3.8 ± 1.9 %, suggesting that about 70% control cells were able to repair membrane damage (**Figure 4b, e and f**). We then examined the response to shear stress after silencing ANXA2 expression. In the presence of Ca^{2+}, 11.3 ± 5.9 % of shANXA2 MDA-MB-231 cells failed to repair their membranes following shear stress, similar to the value for control cells in the absence of Ca^{2+} (**Figure 4c, e and f**). Finally, we examined the ability of an anti-ANXA2 antibody to inhibit membrane repair. We hypothesized that the antibody would enter cells through the disrupted membrane and inhibit membrane repair. Control MDA-MB-231 cells were subjected to shear stress in the presence of both Ca^{2+} and monoclonal anti-ANXA2 antibody. We observed 8.7 ± 3.0 % of unrepaired cells, significantly more than the value for control cells damaged in the presence of Ca^{2+}, and inferred that the presence of anti-ANXA2 antibody leads to a defect in membrane repair after shear stress (**Figure 4d-f**). We conclude that ANXA2 is a crucial component in response to shear stress and that anti-ANXA2 antibodies can inhibit membrane repair despite being administered outside the cell.

MDA-MB-231 cell morphology after membrane damage induced by shear stress

Electron microscopy was used to study the morphology of MDA-MB-231 cells after membrane damage by shear stress in the presence or absence of ANXA2 and Ca^{2+}. Unlike untreated cells (**Figure 5a**), many cells subjected to shear stress in the presence of Ca^{2+} appeared to have lysed (**Figure 5b**). This phenomenon was increased in the absence of Ca^{2+}, suggesting it resulted from membrane damage that was not repaired (**Figure 5c**). In line with this observation, focal membrane damage was frequently observed in cells treated in the presence of Ca^{2+} (**Figure 5d**, **red square**). The absence of spilt cytoplasmic contents indicates that the cells successfully repaired the damage. A large bleb consistently protruded from the site of damage (**Figure 5d, red arrowheads**), as previous observed in skeletal muscle cells[9]. These results indicate that shear stress creates membrane damage, whose repair requires Ca^{2+}, as previously reported for most, if not all, mechanical damage to the plasma membrane[29]. When shANXA2 cells were submitted to the same treatment, we observed that most cells appeared to have lysed, as in the absence of Ca^{2+} (**Figure 5e**). Taken together, these results strongly suggest that shear stress causes membrane damage whose repair requires ANXA2.

ANXA2 deficiency impairs MDA-MB-231 cell invasion

We next addressed the effect of ANXA2 silencing on MDA-MB-231 cell migration using a transwell invasion assay. We allowed cells to migrate through Matrigel or a dense collagen gel

from medium containing 5% FBS in the upper chamber to medium containing 20% FBS in the lower chamber (**Figure 6a and Supplementary Figure 4**). After 24 h of incubation, cells in the lower chamber were stained with crystal violet. In the absence of ANXA2, the number of MDA-MB-231 cells in the lower chamber decreased by 72% and 62% for inserts covered with Matrigel and collagen, respectively (**Figure 6b**). We conclude that ANXA2 deficiency reduces the invasiveness of MDA-MB-231 cells.

ANXA2 is required for metastasis *in vivo* in mice

To investigate the role of ANXA2 in tumor progression, we labelled control and shANXA2 MDA-MB-231 cells with a luciferase reporter and injected the cells into the tail vein of NOD SCID mice (**Figure 7a-b and supplementary Figure 5**) and RAG mice (**Supplementary Figure 6**). The control cells engrafted in the lungs and bones, particularly in the hind legs (**Figure 7a-b and Supplementary Figure 7**). The ANXA2-deficient cells were much less effective at colonizing the lungs and failed to engraft in the bones (**Figure 7a-b and supplementary Figure 6**). To confirm this result, some of NOD SCID mice initially injected with shANXA2 MDA-MB-231 cells, which did not show tumor development after the first injection (**Figure 7b, black arrow**), were injected a second time with control or ANXA2 deficient MDA-MB-231 cells (**Figure 7c-d**). Again, we observed that shANXA2 MDA-MB-231 cells formed fewer metastases in the lungs and bone compared to control cells (**Figure 7c-d**). We conclude that ANXA2 is required for metastasis in mice.

ANXA2 is required for metastasis *in vivo* in zebrafish

To confirm the lower propensity of ANXA2-deficient cells to metastasize, we injected control or shANXA2 MDA-MB-231 cells injected into the yolk sac of zebrafish larvae and quantified metastases formed in the tail and/or head of the fish (**Figure 8a and Supplementary Figure 8**). At 28 hours post-injection (hpi), we observed that the relative growth of the tumor within the yolk sac was much lower after injection of shANXA2 MDA-MB-231 cells compared to control cells, suggesting reduced survival of ANXA2 deficient cells (**Figure 8b**). We also observed that all fish injected with the control cells showed caudal and/or cranial metastases at 28 hpi, compared to 13% for shANXA2 cells injected fish (**Figure 8c**). Finally, we observed that the mortality rate was 86% for fish injected with control cells but only 25% for those injected with ANXA2 deficient cells at 52 hpi (**Figure 8d**). We conclude that ANXA2 is required for engraftment and metastasis in zebrafish.

High expression of ANXA2 in clinical datasets predicts poor prognosis

Finally, to explore the involvement of ANXA2 in promoting cancer progression in humans, we examined whether its expression was correlated with prognosis in various cancers. Kaplan-Meier plots show that high ANXA2 gene expression identifies poor prognosis patients with lung, gastric and ovarian cancer (**Figure 9a**). This was true in the whole population and in subgroups with advanced disease defined by high grade or stage. In breast cancer, high ANXA2 expression was only correlated with poor survival in patients suffering from triple-negative breast cancer (**Figure 9b**). We conclude that poor prognosis tumors express high levels ANXA2 and infer that they do so to cope with high levels of membrane damage, making them excellent candidates for treatments targeting ANXA2.

Discussion

The main conclusion from this study is that efficient repair of membrane damage is required for tumor invasion and metastasis. We hypothesized that cancer cells would require efficient membrane repair to cope with the physical stresses they are exposed to during invasion and metastasis. We confirmed that this is indeed the case using two different animal models in which inhibition of membrane repair drastically reduced the invasion and metastasis of breast cancer cells. To prevent membrane repair we inhibited ANXA2 gene expression and protein function in hormone receptor negative MDA-MB-231 breast cancer cells. The requirement for ANXA2 is independent of the type of membrane damage, since it was seen after laser ablation and shear stress.

In skeletal muscle cells, ANXA2 participates in lipid patch formation where it is recruited to the damaged plasma membrane by interacting with dysferlin[3,22]. The mechanism of membrane repair is best understood in muscle cells. Shearing forces are one of the major mechanical constraints applied to cancer cells during their dissemination[10] but little is known about membrane repair in cancer cells. Since ANXA2 interacts with actin, it could be involved directly in cell migration or proliferation[30], but we show that these processes are largely unaffected in ANXA2-deficient MDA-MB-231 cells. Hence, we propose that defective membrane repair specifically affects invasion and metastasis.

We have shown that ANXA2 is highly expressed in poor prognosis tumors. We speculate that this is an adaptation to survive the membrane damage these tumors suffer during invasion and metastasis. Since normal cells are not exposed to these stresses, we propose that inhibition of membrane repair will disproportionately affect poor prognosis tumours. This means inhibitors of membrane repair should have a high therapeutic index. We show that an

inhibitory antibody against ANXA2 is able to inhibit repair when administered in the culture medium. To affect repair the antibody must enter the cell, and we propose that it does so at sites of membrane damage. Intriguingly, this means therapeutic antibodies should only affect cells with membrane damage, potentially further increasing the therapeutic index. This result confirms a previous report on ovarian cancer cells showing that anti-ANXA2 antibody significantly decreases invasion of the chick embryo chorioallantoic membrane and inhibits tumor growth and metastasis in nude mice[31]. It opens new routes using immunotherapy to tackle cancer cell dissemination. An alternative to antibody therapy would be to use small molecule inhibitors or peptides. Drugs used to treat psychiatric and allergic conditions, such as trifluoperazine, have been reported to inhibit annexin-mediated membrane repair[32], and a synthetic cell-penetrating peptide that interacts with ANXA2 has been shown to reduce metastasis to murine lungs[33]. Major compressive and shearing forces are encountered during invasion and metastasis. We conclude that repair of membrane damage is a new target for cancer therapy that could be used to prevent invasion and metastasis of poor prognosis tumours.

Methods

Ethical issues. Accommodations and experiments were performed in the animal facility ("Service des animaleries") of the University of Bordeaux. Female RAGγ2C−/− (RAG within the manuscript) or NOD SCID mice were housed and treated in the animal facility. RAG mice were obtained from the animal facility of the University of Bordeaux and NOD SCID mice were purchased from Charles River Laboratories (Wilmington, MA, USA). All animal procedures have been done according to the institutional guidelines and approved by the local ethics committee (agreement number: APAFIS#28418-2020110415441210 v7). Adult zebrafishes were produced in our facilities in accordance with the French Directive (Ministère de l'Agriculture et de l'Alimentation) under permit number A33-063-935. All the procedures were conducted in compliance with the European Communities Council Directive (2010/63/EU).

Cell culture. Cell culture media and reagents were from ThermoFisher Scientific (Waltham, MA, USA) except when otherwise stated. MDA-MB-231 human breast tumor cells expressing tdTomato and luciferase proteins were established by lentiviral transduction as previously described[34] using the pDRM18 LTN plasmid (Addgene number 174721). Cells were cultured in Dulbecco modified Eagle's minimal essential medium (DMEM) containing 4 mM Glutamax© and supplemented with 10% fetal bovine serum and penicillin / streptomycin (100 U/mL and 100 µg/mL). Cells were maintained at 37°C in a 5% CO_2 humidified incubator.

Generation of ANXA2 knock-down or knock-out MDA-MB-231 cells. Two complementary strategies were used to generated ANXA2 deficient MDA-MB-231 cells. MDA-MB-231 cells were either transduced with ANXA2-targetting shRNA or an ANXA2-knock-out cell line was established using a CRISPR-Cas9 approach. For the knock-out cell line, a gRNA targeting ANXA2 DNA sequence (5'- TCTCTGTGCATTGCTGCGGT -3') located in exon 3 was designed using CRISPOR algorithm (crispor.tefor.net[35]). Alt-R®-crRNA corresponding to target sequence was purchased from Integrated DNA Technologies (IDT) as well as human crRNA negative control. They were both resuspended to 100 µM in TE buffer and then equally mixed with 100 µM Alt-R®-tracrRNA (IDT), annealed by heating for 5 minutes at 95°C and cooled to room temperature (RT). This dual gRNA was mixed with 5 µg of Alt-R® S.p-Cas9HIFIv3 (IDT) with a 1.2 ratio of gRNA/Cas9. After 10 minutes at RT, 2 x 10^5 MDA-MB-231 cells resuspended in Lonza SE solution were added to the CRISPR mix. Program CH-125 of the 4D-Nucleofector® (Lonza) was applied. Two or three days after transfection, cells were

trypsinized and half of them were cultured while the other half was pelleted, lysed and used as PCR template using Phire Tissue Direct PCR Master Mix (ThermoFisher Scientific). PCR amplification of the targeted area was done following supplier instructions with primers 5'-TGGGTAGAGGATGCTGACGA-3' and 5'-CAGAAGCTCTCCCTCCAGGT-3'. Sequencing of PCR products was done by Eurofins Genomics and Sanger data were analyzed to quantify Indels reflecting gene KO with DECODR algorithm (decodr.com[36]) or ICE algorithm (ice.synthego.com[37]). Cells were diluted and seeded to 0.5 cell/well in 96 well plates and let to expand to obtain cellular clones, which were then characterized by Sanger sequencing and western blot analysis. Regarding the shRNA strategy, the following sequences, which were cloned into the pLKO.1 puro-vector (MISSION® shRNA plasmids, Sigma-Aldrich, Saint-Louis, MO, USA), was used: ANXA2-targetting shRNA: 5'-CCGGCGGGATGCTTTGAACATTGAACTCGAGTTCAATGTTCAAAGCATCCCGTTTTTG-3'; control shRNA: 5′-CCTAAGGTTAAGTCGCCCTCGCTCGAGCGAGGGCGACTTAACCTTAGG-3′. Lentiviral-based particles containing shRNA were produced by Bordeaux University Lentiviral Vectorology Platform (US005, Bordeaux, France) by transient transfection of 293T cells. 2.10^5 MDA-MB-231 cells were cultured in a 30 mm Petri Dish for 24 h and transduction was carried out by adding concentrated lentiviral particles to the cells at multiplicity of infection (MOI) of 10 in 2 mL Opti-MEM® for 24 h. Transduced cells were cultured for 24 h in growth medium and then selected in selection medium composed by 2 µg/mL puromycin in DMEM for 48 h. Cells were passed and subsequently cultured in 25 cm² cell culture flask in selection medium. At each passage, a fraction of cells was used for preparing protein extracts for western-blot analysis of the expression of endogenous ANXA2. All the experiments were performed with shANXA2 MDA-MB-231 cells. Membrane repair assays using laser ablation and shear-stress assays were in addition performed with ANXA2-KO MDA-MB-231 cells and led to similar results to those obtained with shANXA2 MDA-MB-231 cells.

Western-blot. 2.10^6 cells were trypsinized, pelleted and re-suspended in 300 µL of D-PBS supplemented with 1 mM EGTA. Protein extracts were obtained by sonicating ice-cold cell suspension with a Branson digital sonifier (amplitude 20%, duration 2 min, interval 5 s and pulse 5 s). Two successive centrifugations at 13,000g for 1 min allowed to remove cell debris. 10 µg protein extracts were separated on a 10% SDS-PAGE. Semi-dry electrophoretic transfer (Bio-Rad, Hercules, CA, USA) onto PVDF membrane was performed for 1 h at 100 V. The cellular content in ANXA1 (37 kDa), ANXA2 (36 kDa), ANXA4 (35 kDa), ANXA5 (35 kDa),

ANXA6 (68 kDa), and actin (42 kDa) or GAPDH (37 kDa) was detected with rabbit anti-ANXA1 polyclonal antibody (PA1006, BosterBio, Pleasanton, CA, USA), mouse anti-ANXA2 monoclonal antibody (3E8-B6, Sigma-Aldrich), mouse anti-ANXA4 monoclonal antibody (SAB4200121, Sigma-Aldrich), mouse anti-ANXA5 monoclonal antibody (AN5, Sigma-Aldrich), mouse anti-ANXA6 monoclonal antibody (sc-271859, Santa cruz Biotechnology, Dallas, USA), rabbit anti-actin polyclonal antibody (A2066, Sigma-Aldrich), and rabbit anti-GAPDH polyclonal antibody (G9545, Sigma-Aldrich), respectively. Except for anti-actin and anti-GAPDH antibodies (1:5,000), all primary antibodies were used at 1:1,000 dilution in saturation solution composed by Tris buffer saline (10 mM Tris, 150 mM NaCl, pH 8.0) supplemented with 0.1% Tween20 and 5% non-fat dry milk. Revelation was performed using secondary antibodies conjugated to horse-radish peroxidase (GE-Healthcare, Chicago, USA) diluted 1:2,000 in saturation solution and Opti-4CN™ colorimetric kit (Bio-Rad). ImageJ software was used to measure the relative intensity of protein bands.

Membrane rupture and repair assay. Membrane repair assay was performed as previously described[17]. MDA-MB-231 cells were irradiated at 820 nm with a tunable pulsed depletion laser Mai Tai HP (Spectra-Physics, Irvine, USA) of an upright two-photon confocal scanning microscope (TCS SP5, Leica, Wetzlar, Germany) equipped with an HCX PL APO CS 63.0 x 1.40 oil-objective lens. Irradiation consisted of 1 scan (1.6 s) of a 1 µm x 1 µm area with a power of 110 (±5) mW. 512 x 512 images were acquired at 1.6 s intervals with pinhole set to 1 Airy unit. FM1-43 was excited by the 488-nm laser line (intensity set at 20% of maximal power) and fluorescence emission was measured between 520 nm and 650 nm. For quantitative analysis, the fluorescence intensity was integrated over the whole cell surface and corrected for the fluorescence value recorded before irradiation, using ImageJ software.

Traffic of ANXA2 in laser-injured cells. For subcellular localization of endogenous ANXA2 in damaged MDA-MB-231 cells, cells were cultured in 35-mm glass bottom dishes equipped with a square patterned coverslip (MatTek, Ashland, USA) and membrane rupture was performed according to the protocol described above, but in the absence of FM1-43 to avoid fluorescence cross-talk. After laser irradiation, cells were fixed in 1% glutaraldehyde and permeabilized in 0.1% TritonX100 diluted in DPBS+Ca^{2+}. All subsequent steps (saturation, antibody incubation and washes) were performed using 2% BSA in DPBS+Ca^{2+} solution. Primary mouse anti-ANXA2 monoclonal antibody (1:100, 3E8-B6, Sigma-Aldrich) and secondary Alexa Fluor 488-coupled anti-mouse IgG goat antibody (1:1000, ThermoFisher

Scientific) were successively incubated with cells for 1 h at 37°C. Finally, cells were washed in DPBS+Ca^{2+} and nuclear counterstaining was performed with DAPI (Sigma-Aldrich). For each condition, about 30 cells from three independent experiments were analyzed. For the subcellular trafficking analysis of ANXA2-GFP, shANXA2 MDA-MB-231 cells cultured in 35-mm glass bottom dishes (MatTek, Ashland, USA) were transfected with the pA2-GFP plasmid[38], as previously described[9]. Membrane damage was performed by laser ablation as described above, without FM1-43. At least three independent experiments were performed and each experiment included the analysis of at least five damaged cells.

2-D Migration assay. 6-well clear plates (Corning, NY, USA) were coated with gelatin 0.5 mg/mL (Sigma-Aldrich) and incubated for 20 min at 37°C. Gelatin was crosslinked by incubation with glutaraldehyde 0.5% (Sigma-Aldrich) for 40 minutes at 37°C. A 2-chamber culture-insert (Ibidi, Gräfelfing, Germany) was placed in the center of each well. 3 x 10^4 cells in 1 mL of complete growth medium was added in the well and each culture-insert chamber was filled with 2 x 10^3 cells in 70 µL growth medium and incubated at 37°C, 5% CO_2. The culture-insert was then carefully removed and 2 ml of complete growth medium were added into the well. Quantitative phase images were acquired with a lens-free microscope (Cytonote, Iprasense, Montpellier, France) in an incubator at 37°C, 5% CO_2. The acquisition period was 20 minutes. Analysis was performed on ImageJ using the MRI Wound Healing Tool.

Proliferation analysis

6-well clear plates (Corning) were coated with gelatin as described for migration assay. 1.6 x 10^5 cells/well were seeded in duplicate in growth medium without red phenol to avoid disturbance of the phase measurement. Quantitative phase images were acquired with a lens-free microscope (Cytonote, Iprasense, Montpellier, France) in an incubator at 37°C, 5% CO_2. The acquisition period was 25 minutes. Three independent experiments were performed for each cell line.

Fluid shear-stress assay. Adherent control or shANXA2 MDA-MB-231 cells were collected at 80% confluence after incubation with 0,25% trypsin (Gibco) in 5% CO_2 at 37°C and 5 x 10^5 cells were suspended in 1 mL of growth medium in a Falcon™ polystyrene tubes (Corning). At this stage either Ca^{2+} (Final concentration 2 mM), or 2 mM EGTA, or mouse anti-ANXA2 monoclonal antibody (1:100, 3E8-B6, Sigma-Aldrich) supplemented with Ca^{2+} (Final concentration 2 mM) was added to the medium. The suspension was slowly loaded into a 1 ml

syringe (Becton Dickinson, NJ, USA), which was subsequently equipped with a 30G needle (Terumo, Tokyo, Japan). Then, the suspension was gently expelled against the wall of the polystyrene tube at room temperature at a constant flow rate either via an automated NeMESYS syringe pump (200 µL/s, Cetoni GmbH, Korbussen, Germany) or manually. The load/expel cycle was repeated 10 times. 10 min after the treatment, 50 µL of the cell suspension were put into a 96-well plate and 4 µg/mL DAPI was added in order to stain damaged cells. As a control condition, cells in growth medium with Ca^{2+} (Final concentration 2 mM) were incubated with 4 µg/mL DAPI without to be submitted to shear stress (no-stress condition). Cell imaging of tdTomato (all cells) and DAPI (unrepaired cells) was performed as described in the Fluorescence microscopy section. Images were analyzed with ImageJ software.

3-D invasion assay

Transwell chambers (8.0µm pore size, Falcon 353097) were coated with 150µl of Matrigel (80µg/ml) or fibrillar collagen (0.5mg/ml) in a 24-well plate. For each condition, 40,000 MDA-MB-231 cells (control or shANXA2) per transwell were seeded in complete medium with 5% of FBS. As a chemoattractant, 20% FBS complete medium was used in the lower part of the transwell in the 24-well plate. After 24 h, the media was carefully removed, cells were fixed with 4% PFA for 10 min and stained with crystal violet (Sigma-Aldrich) for 20 minutes at room temperature. Cells in the upper part of the transwell membrane were removed by wiping with a cotton swab. A phase-contrast microscope (Zeiss) was used to image migrated cells in the lower chambers, 10 images per condition and per replicate were acquired. Three independent experiments were performed. Images were analyzed using ImageJ software.

Fluorescence microscopy. Cell imaging was performed using a conventional fluorescence microscope IX81 (Olympus, Tokyo, Japan) equipped with a UPLFLN20X/0.50/WD2.1mm and a UPLFLN60XO/0.65/0.65-1.25/D0.12 objectives. DAPI and Hoechst were observed using the U-MWU2 cube containing a band-pass excitation filter (330-385 nm), a dichroic mirror (threshold 400 nm) and a long-pass emission filter (threshold 420 nm). GFP and Alexa488 were observed using the U-MINIBA2 cube containing a band-pass excitation filter (470-490 nm), a dichroic mirror (threshold 505 nm), and a band-pass emission filter (510-550 nm). tdTomato was observed using the cube U-MWG2 containing a band-pass excitation filter (510-550 nm), a dichroic mirror (threshold 570 nm) and a long-pass emission filter (threshold 590 nm).

Transmission electron microscopy

5.10^5 cells submitted or not to shear stress assay were centrifuged at 200 g for 5 min in a 1.5 mL polypropylene tube. The pellet was incubated with a solution of Karnovsky fixative at 4°C overnight. The pellet was washed with 0.1 M sodium cacodylate buffer (Agar Scientific, Stansted, UK), then post-fixed for 1 h in 1% osmium tetroxide (Agar Scientific) in sodium cacodylate buffer and then washed three times and finally re-suspended in 20 µL of cacodylate buffer. A 5 µL drop was introduced into the core of a warm (40°C-50°C) 8% agarose fluid gel in a 1.5 mL polypropylene tube. Once solidified, a 3 mm^3 block is cut around the drop. Dehydration process was performed by 3 successive baths of 10 min in 100% ethanol followed by incubation in propylene oxide. The sample was then embedded in Epon-Araldite and ultra-thin sections (65 nm with Leica EM-UC6 ultra-microtome) were stained for 10 min in 5% uranyl acetate and 5 min in lead citrate. The sections were imaged with a FEI CM120 transmission electron microscope at 120 kV, using a Gatan USC1000-SSCCD camera.

MDA-MB-231 dissemination in mice. MDA-MB-231 cells expressing the luciferase protein, either wild-type or ANXA2 deficient, were trypsinized and washed with PBS twice. Female RAG or NOD SCID mice (8-12 weeks old) were anaesthetized with 2% isoflurane. 10^6 cells in 0.1 ml PBS were injected into the lateral tail vein using a 27 ½ gauge needle. For bioluminescence imaging, intraperitoneal injection of d-Luciferin (150 mg/kg) was performed. The mice were immediately placed onto a black pad in the Photon Imager™ (BIOSPACE, Paris, France) box and imaged ventrally. Animals were imaged 30 min after cell injection and then once a week for at least 5 weeks. For image acquisition, unit was set to ph/cm^{-2}/s^{-1}/sr^{-1}. To quantify the signal, a region of interest was chosen as a circle of 13 cm² centered either on lungs or the hindquarters of the mouse.

MDA-MB-231 dissemination in zebrafish

Experiments were performed using the Casper zebrafish stain (ZIRC, Oregon, USA). Adult fish aged 6 months to 2 years were crossed to produce embryos. Embryos were cultured in E3 medium (5 mM NaCl, 0.17 mM KCl, 0.33 mM $CaCl_2$, 0.33 mM $MgSO_4$) at 28°C. Dechorionated 2-day post fertilization (dpf) zebrafish embryos were anaesthetized with 0,003% tricaine/ (Sigma-Aldrich) and positioned in 3% methylcellulose on a dish coated with 1% agarose. MDA-MB-231 cells expressing the tdTomato protein, either wild-type or ANXA2 deficient, were treated with versene solution and resuspended in PBS containing 1% phenol red at the density of 4 x 10^7 cells per mL. The cell suspension was loaded into borosilicate glass

capillary needles (Femtotip II, Eppendorf, Hamburg, Germany) and injections were performed using a pump (Femtojet 4i; Eppendorf) and micromanipulator (Phymep, Paris, France). Around 500 cells/embryos were injected above the duct of cuvier in perivitelline space of the embryo. After checking the implantation with mammalian cells, zebrafish embryos were maintained at 35,5°C. Tumor imaging is done at 3-, 28- and 52-hour post injection (hpi).

Immunohistochemistry

Murine lungs were fixed in PFA 4% for 48 h at 4°C progressively dehydrated in ethanol, incubated in toluene and embedded in paraffin. Five micrometer sections were stained with hematoxylin/eosin or used for immunostaining. For immunostaining, sections were deparaffinized in toluene, rehydrated gradually in ethanol and rinsed in dH2O. Slides were permeabilized 15 min in 0.1% TritonX100 and saturated 1 hour in 5% BSA in PBS. Anti-tdTomato primary antibody (1:50, DsRed (E-8), Santa cruz Biotechnology) was dissolved in 1% BSA in PBS and incubated overnight at 4°C. After washes, slices were incubated with secondary Alexa Fluor 488-coupled anti-mouse IgG goat antibody (1:500, ThermoFisher Scientific) for 1 hour at RT. Hoechst at 2 µg/mL in PBS and incubated 5 min at RT. Slices were mounted in ProLong medium and dry at RT before imaging.

Survival analysis. The Kaplan–Meier plotter database (https://kmplot.com/analysis/)[39] was used to correlate overall survival rate to the level of ANXA2 mRNA expression. To determine the prognostic value of ANXA2, patients were split by auto-selecting the best cutoff, the period of follow-up was fixed at 120 months, the "only JetSet best probe set" option was selected, and biased arrays was excluded. Hazard ratios with 95% confidence interval and log-rank P value were calculated. The log-rank test calculates the mean chi-square for each event time from each group. Two groups are considered to be significantly different when $P < 0.05$.

References

1. McNeil & Steinhardt, R. A. Plasma membrane disruption: repair, prevention, adaptation. *Annu. Rev. Cell Dev. Biol.* **19**, 697–731 (2003).
2. Bansal, D. *et al.* Defective membrane repair in dysferlin-deficient muscular dystrophy. *Nature* **423**, 168–172 (2003).
3. Lennon, N. J. *et al.* Dysferlin interacts with annexins A1 and A2 and mediates sarcolemmal wound-healing. *J. Biol. Chem.* **278**, 50466–50473 (2003).

4. Bouter, A. *et al.* Annexin-A5 assembled into two-dimensional arrays promotes cell membrane repair. *Nat. Commun.* **2:270**, 270 (2011).
5. Boye, T. L. *et al.* Annexin A4 and A6 induce membrane curvature and constriction during cell membrane repair. *Nat. Commun.* **8**, 1623 (2017).
6. Gerke, V. & Moss, S. E. Annexins: from structure to function. *Physiol. Rev.* **82**, 331–371 (2002).
7. Carmeille, R. *et al.* Annexin-A5 promotes membrane resealing in human trophoblasts. *Biochim. Biophys. Acta* **1853**, 2033–2044 (2015).
8. Carmeille, R. *et al.* Membrane repair of human skeletal muscle cells requires Annexin-A5. *Biochim. Biophys. Acta - Mol. Cell Res.* **1863**, 2267–2279 (2016).
9. Croissant, C., Gounou, C., Bouvet, F., Tan, S. & Bouter, A. Annexin-A6 in Membrane Repair of Human Skeletal Muscle Cell: A Role in the Cap Subdomain. *Cells* **9**, 1742 (2020).
10. Wirtz, D., Konstantopoulos, K. & Searson, P. C. The physics of cancer: the role of physical interactions and mechanical forces in metastasis. *Nat. Rev. Cancer* **11**, 512–522 (2011).
11. Azevedo, A. S., Follain, G., Patthabhiraman, S., Harlepp, S. & Goetz, J. G. Metastasis of circulating tumor cells: favorable soil or suitable biomechanics, or both? *Cell Adh. Migr.* **9**, 345–356 (2015).
12. Gensbittel, V. *et al.* Mechanical Adaptability of Tumor Cells in Metastasis. *Dev. Cell* **56**, 164–179 (2021).
13. Lauritzen, S. P., Boye, T. L. & Nylandsted, J. Annexins are instrumental for efficient plasma membrane repair in cancer cells. *Semin. Cell Dev. Biol.* **45**, 32–38 (2015).
14. Sakwe, A. M., Koumangoye, R., Guillory, B. & Ochieng, J. Annexin A6 contributes to the invasiveness of breast carcinoma cells by influencing the organization and localization of functional focal adhesions. *Exp. Cell Res.* **317**, 823–837 (2011).
15. Leung, C., Yu, C., Lin, M. I., Tognon, C. & Bernatchez, P. Expression of myoferlin in human and murine carcinoma tumors: role in membrane repair, cell proliferation, and tumorigenesis. *Am. J. Pathol.* **182**, 1900–9 (2013).
16. Uhlen, M. *et al.* A pathology atlas of the human cancer transcriptome. *Science* **357**, eaan2507 (2017).
17. Bouvet, F. *et al.* Defective membrane repair machinery impairs survival of invasive cancer cells. *Sci. Rep.* **10**, 21821 (2020).
18. Mahdi, A. F. *et al.* Expression of Annexin A2 Promotes Cancer Progression in

Estrogen Receptor Negative Breast Cancers. *Cells* **9**, 1582 (2020).

19. Daubon, T. *et al.* Deciphering the complex role of thrombospondin-1 in glioblastoma development. *Nat. Commun.* **10**, 1146 (2019).
20. Hogarth, M. W. *et al.* Fibroadipogenic progenitors are responsible for muscle loss in limb girdle muscular dystrophy 2B. *Nat. Commun.* **10**, 2430 (2019).
21. Bittel, D. C. *et al.* Annexin A2 Mediates Dysferlin Accumulation and Muscle Cell Membrane Repair. *Cells* **9**, 1919 (2020).
22. Croissant, C., Carmeille, R., Brévart, C. & Bouter, A. Annexins and membrane repair dysfunctions in muscular dystrophies. *Int J Mol Sci* **22**, 5276 (2021).
23. Koerdt, S. N. & Gerke, V. Annexin A2 is involved in Ca2+-dependent plasma membrane repair in primary human endothelial cells. *Biochim. Biophys. Acta - Mol. Cell Res.* **1864**, 1046–1053 (2017).
24. Jaiswal, J. K. *et al.* S100A11 is required for efficient plasma membrane repair and survival of invasive cancer cells. *Nat. Commun.* **5**, 3795 (2014).
25. Thompson, E. W. *et al.* Differential regulation of growth and invasiveness of MCF-7 breast cancer cells by antiestrogens. *Cancer Res.* **48**, 6764–8 (1988).
26. Thompson, E. W. *et al.* Association of increased basement membrane invasiveness with absence of estrogen receptor and expression of vimentin in human breast cancer cell lines. *J. Cell. Physiol.* **150**, 534–44 (1992).
27. Carmeille, R., Croissant, C., Bouvet, F. & Bouter, A. Membrane repair assay for human skeletal muscle cells. *Methods Mol. Biol.* **1668**, 195–207 (2017).
28. Croissant, C., Bouvet, F., Tan, S. & Bouter, A. Imaging Membrane Repair in Single Cells Using Correlative Light and Electron Microscopy. *Curr Protoc Cell Biol* **81**, e55 (2018).
29. Corrotte, M., Castro-Gomes, T., Koushik, A. B. & Andrews, N. W. Approaches for plasma membrane wounding and assessment of lysosome-mediated repair responses. *Methods Cell Biol.* **126**, 139–158 (2015).
30. Hayes, M. J., Shao, D., Bailly, M. & Moss, S. E. Regulation of actin dynamics by annexin 2. *EMBO J.* **25**, 1816–26 (2006).
31. Lokman, N. A. *et al.* Annexin A2 is regulated by ovarian cancer-peritoneal cell interactions and promotes metastasis. *Oncotarget* **4**, 1199–1211 (2013).
32. Heitmann, A. S. B. *et al.* Phenothiazines alter plasma membrane properties and sensitize cancer cells to injury by inhibiting annexin-mediated repair. *J. Biol. Chem.* **297**, 101012 (2021).

33. Staquicini, D. I. *et al.* Intracellular targeting of annexin A2 inhibits tumor cell adhesion, migration, and in vivo grafting. *Sci. Rep.* **7**, 4243 (2017).
34. Iggo, R. Lentiviral Transduction of Mammary Epithelial Cells. *Methods Mol. Biol.* **2471**, 159–183 (2022).
35. Haeussler, M. *et al.* Evaluation of off-target and on-target scoring algorithms and integration into the guide RNA selection tool CRISPOR. *Genome Biol.* **17**, 148 (2016).
36. Bloh, K. *et al.* Deconvolution of Complex DNA Repair (DECODR): Establishing a Novel Deconvolution Algorithm for Comprehensive Analysis of CRISPR-Edited Sanger Sequencing Data. *Cris. J.* **4**, 120–131 (2021).
37. Conant, D. *et al.* Inference of CRISPR Edits from Sanger Trace Data. *Cris. J.* **5**, 123–130 (2022).
38. Croissant, C., Gounou, C., Bouvet, F., Tan, S. & Bouter, A. Trafficking of Annexins during Membrane Repair in Human Skeletal Muscle Cells. *Membranes (Basel).* **12**, 153 (2022).
39. Lánczky, A. & Győrffy, B. Web-Based Survival Analysis Tool Tailored for Medical Research (KMplot): Development and Implementation. *J Med Internet Res* **23**, e27633 (2021).
40. Allier, C. *et al.* Imaging of dense cell cultures by multiwavelength lens-free video microscopy. *Cytom. Part A* **91**, 433–442 (2017).
41. Clarke, M. S. F. & McNeil, P. L. Syringe loading introduces macromolecules into living mammalian cell cytosol. *J. Cell Sci.* **102**, 533–541 (1992).

Acknowledgments

This work was funded by la Ligue Contre Le Cancer de Gironde (grant 191796 and 238171 to A.B.) and Ligue Contre Le Cancer du Lot-et-Garonne (grant 238294 to A.B.). Christel Poujol and Sébastien Marais are acknowledged for the help in membrane repair assays that were done in the Bordeaux Imaging Center a service unit of the CNRS-INSERM and Bordeaux University, member of the national infrastructure France BioImaging supported by the French National Research Agency (ANR-10-INBS-04). The authors thank the staff of Vect'UB and CRISPR-edit technology platforms (INSERM US 005 – CNRS UAR 3427- TBM-Core, University of Bordeaux, France) for technical assistance. The authors would like to thank Marie Paul Algeo and Marcia Campistron for her assistance in the animal facility. The authors thank Christine Varon for her help in KMplotter analysis.

Author contributions

C.G., F.B. and A.B. performed the majority of experiments with assistance from L.A. (western-blot analysis and shear-stress assays), D.C. (shear-stress assays), L.R. and F.S. (3D invasion assay), V.P.M. (establishment of koANXA2 MDA-MB-231) S.T. (electron microscopy), L.B., G.S. and M.K. (zebrafish experiments), M.M, E.H. and F.A. (proliferation and 2D migration assays), W.S. (mouse experiments), R.I. (establishment of luc+/tdTomato+ MDA-MB-231 cells). A.B. coordinated the entire project and designed the experiments, with the help of A.R.B and R.I.. A.B., A.R.B. and R.I. wrote the manuscript. L.A., F.A., E.H., G.S., M.K. contributed to the writing of the manuscript.

Additional information

Supplementary Information accompanies this paper at http://www.nature.com/naturecommunications

Competing financial interests: The authors declare no competing financial interests.

Figure legends

Figure 1: Invasiveness properties of breast cancer cells are correlated with high expression of ANXA1 and ANXA2. a Representative image of western-blot analysis showing the revelation of ANXA2 in MDA-MB-231 and MCF7 cells, compared to GAPDH (loading control). **b** The histogram presents mean values (± SEM) of the ratio ANX/GAPDH from five independent experiments, analyzed by the gel analysis plugging of ImageJ. A representative membrane of the detection of ANXA1 is presented in supplementary Figure 1. Student t-test for independent samples. **: $p < 0.01$.

Figure 2: ANXA2 is required for membrane repair in MDA-MB-231 cells. a ANXA2 deficient MDA-MB-231 cells was generated by shRNA transduction strategy. The cellular content of ANXA2 in MDA-MB-231 cells transduced with lentiviral particles containing shRNA targeting ANXA2 (shA2) or a scrambled shRNA (ctl) was quantified by Western blotting. The expression of ANXA2 is decreased of more than 90% in shANXA2 MDA-MB-231 cells. **b** Control and shANXA2 MDA-MB-231 cells, which expressed constitutively the tdTomato fluorescent protein were imaged by fluorescence microscopy. **c, e** Sequences of representative images showing the response of a control (c) or shANXA2 (e) MDA-MB-231 cell to a membrane damage performed by 110-mW infrared laser irradiation, in the presence of FM1-43 (green). In all figures, the area of membrane irradiation is marked with a red arrow before irradiation and a white arrow after irradiation. Scale bars: 10 µm. **d** Kinetic data represent the FM1−43 fluorescence intensity integrated over whole cell sections, averaged for about 30 cells (+/−SEM). For a majority of control MDA-MB-231 cells, the fluorescence intensity reached a plateau after about 80 s (black filled circles). For shANXA2 MDA-MB-231 cells, a continuous and large increase of the fluorescence intensity was observed (empty circles), indicating the absence of membrane resealing. **f** Recruitment of ANXA2 to the site of membrane injury. MDA-MB-231 cells transfected with the plasmid pA2-GFP were damaged by laser ablation. Red arrow, area before irradiation; white arrow, area after irradiation. **g** Subcellular localization of endogenous ANXA2 in damaged MDA-MB-231. MDA-MB-231 cells were irradiated with a 110-mW infrared laser (white arrow) in DPBS + Ca^{2+}, then fixed and immunostained for ANXA2 and counterstained with DAPI (blue). After laser injury, MDA-MB-231 cells exhibited an accumulation of ANXA2 at the disruption site. Scale bars: 10 µm.

Figure 3: Proliferation and 2D-migration of MDA-MB-231 cells are independent from ANXA2. a-b Proliferation of control or shANXA2 MDA-MB-231 cells was monitored with a lensfree microscope enabling continue observation of a large cell population[40]. One image was acquired every 25 min. Phase images were analyzed using Trackmates2 on Fiji and MATLAB. **a** Averaged number of cells (+/- SEM) normalized to the number of seeded cells from three independent experiments. **b** Normalized total cell biomass (+/- SEM), which considers individual number and cell size, from three independent experiments. **c-d** *In vitro* 2D-migration assay was performed on control or shANXA2 MDA-MB-231 cells. 3.5 x 10^5 cells/well were plated into culture-Insert 2-well in 35 mm µ-Dish (Ibidi) coated with 0.5 mg/mL gelatin. Cell progression was monitored with a lensfree microscope[40], after removing the culture insert. **c** Typical images of control or shANXA2 MDA-MB-231 cells immediately or 7h after insert release are presented. Migration front is drawn in yellow. **d** Mean gap closure kinetics and cell velocity measure (+/- SEM) from three independent experiments are presented for each cell type. Non-parametric Mann-Whitney test. ***: $p < 0.001$.

Figure 4: Response of control or shANXA2 MDA-MB-231 cells to membrane injury by shear-stress treatment. a Scheme of the protocol with a photography of the device used for the automatized shear-stress treatment. The microfluidic approach is based on a method initially devoted to introduce large macromolecules into mammalian cells[41]. 5 x 10^5 cells/mL cells were loaded in a 1 mL syringe with a 30G needle mounted on a fully automated NeMESYS syringe pump system (Cetoni GmbH, Korbussen, Germany). After 10 passages through the needle, cells were incubated with DAPI, which stained damaged/unrepaired cells, while all cells expressed the fluorescent protein tdTomato. Created using Biorender.com. **b** Representative images of control unstressed MDA-MB-231 (left-hand panels), and stressed cells in the absence (middle panels) or presence (right-hand panels) of 2 mM Ca^{2+}. Scale bar: 50 µm for all images. **c** Representative images of shANXA2 MDA-MB-231 submitted to the shear stress assay in the presence of 2 mM Ca^{2+}. Scale bar: 50 µm. **d** Representative images of control MDA-MB-231 submitted to shear stress assay in the presence of 2 mM Ca^{2+} and monoclonal anti-ANXA2 antibody (1:50, Sigma-Aldrich). Scale bar: 50 µm. **e** Unrepaired cells, which are defined as DAPI-positive cells over the whole cell population (tdTomato-positive), were quantified for at least 6 independent experiments. Experimental data together with mean (+/- SEM) are presented. Non-parametric Mann-Whitney test. ** P value (<0.01), *** P value (<0.001), **** P value (<0.0001)**. f** Mean percentage of unrepaired cells represented in e are indicated in the second column. Mean percentage of "repaired cells over the whole cell population" (column 3)

is calculated by subtracting the "unrepaired / whole cell population" rate to 13.6 %, which corresponds to the rate of damaged and unrepaired cells in the absence of Ca^{2+} that prevents membrane resealing. In column 3, SD is calculated according to the formula: SD(X+Y) = SQUARE ROOT(SD(X)²/Nx + SD(Y)²/Ny), where X and Y are two variables, SD the standard deviation of the variable, and Nx/y the number of data for each variable. "Repaired / damaged population" rate (column 4) is calculated as the percentage of repaired cells considering that the number of damaged cells is 13.6.

Figure 5: control and shANXA2 MDA-MB-231 cells submitted to the shear-stress treatment analyzed by TEM. Control cells submitted (b-d) or not (a) to the shear-stress treatment were fixed and embedded in Epon-Araldite. Ultra-thin sections were stained and imaged by TEM. Shear-stress treatment was performed with (b, d and e) or without (c) 2 mM Ca^{2+}. **a** In the absence of treatment, the cells appear with an electron-dense cytoplasmic content and a conspicuous cell membrane. **b** The shear-stress treatment led frequently to the observation of cells stripped of their content (red dotted line). **c** In the absence of Ca^{2+}, this effect was accentuated (cells with red dotted line). **d** In the presence of Ca^{2+}, many cells exhibited isolated micrometric membrane damage (red square), which seemed to be resealed. The right-hand image displays a high-magnification of the area present within the red square. Red arrowheads point out the large bleb protruded from the site of damage. **e** Most shANXA2 MDA-MB-231 cells submitted to the shear-stress treatment appeared to have lysed (red dotted line) in the presence of Ca^{2+}.

Figure 6: ANXA2 deficiency impairs MDA-MB-231 cell invasion. a A Matrigel or dense collagen gel was produced into a transwell and cells were seeded in media with 5% FBS on top of the gel. As chemoattractant, 20% FBS-containing medium was added in the bottom of the well to allow cell invasion through the gel. Created using Biorender.com. **b** Number of control or shANXA2 MDA-MB-231 cells able to cross the gel was quantified. Unpaired Student t-test. ****: $p < 0.0001$.

Figure 7: Genetic inhibition of ANXA2 prevents tissue colonization of MDA-MB-231 cells in NOD SCID mice. a Control or shANXA2 MDA-MB-231 cells were injected in NOD SCID mice as described in the legend of the Supplementary Figure 5. Representative bioluminescence images of NOD SCID mice 30 min (D0) or 70 days (D70) after injection of MDA-MB-231 cells are presented. **b** Bioluminescence quantification in lungs and bone for control (n =5) or

shANXA2 (n = 5) MDA-MB-231 cells. The black arrow points the time when some mice (n = 4), initially injected with shANXA2 MDA-MB-231 cells and exhibiting low signal in bioluminescence imaging, were injected with control (n = 2) or ANXA2 shRNA (n = 2) MDA-MB-231 cells. **c** Representative bioluminescence images of NOD SCID mice, initially injected with shANXA2 MDA-MB-231 cells and, injected a second time with either control or shANXA2 MDA-MB-231 cells, at 30 min (D0) or 76 days (D76) after the second injection. **d** Bioluminescence quantification in lungs and bone for control (n = 2) or shANXA2 (n = 2) MDA-MB-231 cells after the second injection.

Figure 8: Genetic inhibition of ANXA2 prevents invasion and metastasis processes of MDA-MB-231 cells in zebrafish. a Control (n = 21) or shANXA2 MDA-MB-231 (n = 24) cells were injected in the perivitelline space of Casper zebrafish embryos. Tumor imaging was done by fluorescence microscopy at 3-, 28- and 52 hpi through the tdTomato fluorescent protein constitutively expressed in MDA-MB-231 cells. Inset displays magnified image of a portion of the tail with metastases (white arrows). **b** The relative tumor size within the perivitelline space has been measured in embryos either injected by control or shANXA2 cells. **c** The percentage of embryos, which presented caudal or head metastases was quantified at 28 hpi. **d** Mortality rate was calculated at 52 hpi.

Figure 9: High ANXA2 expression in cancer patients is a factor of poor prognosis. Survival curves from Kaplan-Meier plot profiles[39] for lung, gastric, ovarian and breast cancer patients stratified by high and low expression of ANXA2 mRNA (Affymetrix identifier, 201590_x_at). Analysis was performed either over the whole patient population or patients suffering from advanced cancer, characterized by high grade and/or stage. To note, cancer grade (typically numbered from 1 to 3) correlates with the velocity of the disease development while stage (from 1 to 4) characterizes the extent of affected tissues. High-grade and -stage cancers are often very aggressive, with strong tumor invasion and the presence of metastatic cells, respectively. In each analysis, hazard ratio (HR) and log-rank probability were calculated. A HR significantly different from 1 means that survival was better in one of both groups. For example, if a HR is 1.5, the survival probability in group 1 is 1.5 higher than in group 2. **a** Survival curves for lung (n = 1925), ovarian (n = 1656) or gastric (n = 875) cancers within the whole patient population (whole, first row) or patients suffering from advanced cancer (advanced, second row). Advanced cancers were grade 3, stage 3 + grade 3, and stage N > 1 + M = 1, for lung (n = 77), ovarian (n = 744) and gastric (n = 51) cancer, respectively. **b** Survival curves for the whole

breast cancer patients (n = 1879) or those with an advanced disease (stage N = 3; n = 586). Triple-negative is an invasive and aggressive form of breast cancer that is estrogen receptor-negative, progesterone receptor-negative, and HER2-negative.

Figures

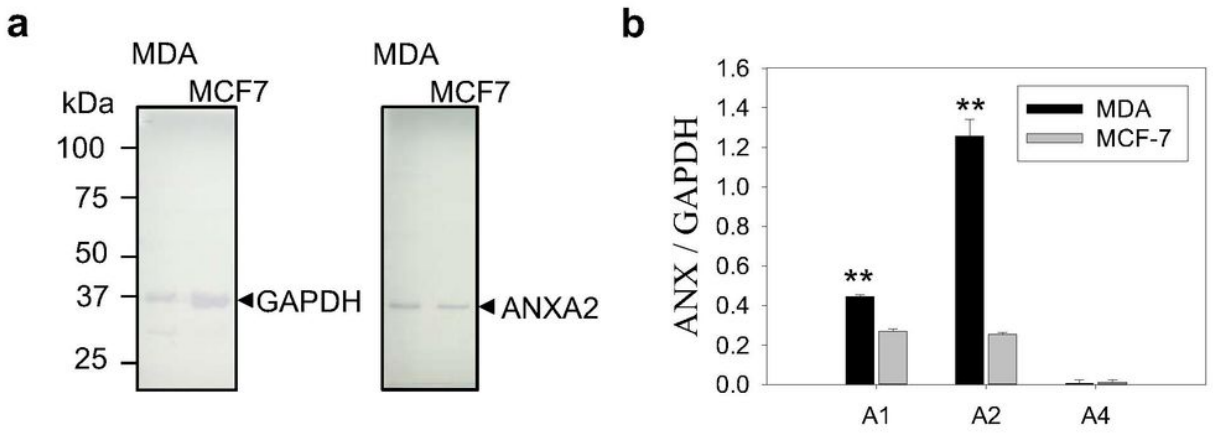

Figure 1

Invasiveness properties of breast cancer cells are correlated with high expression of ANXA1 and ANXA2. a Representative image of western-blot analysis showing the revelation of ANXA2 in MDA-MB-231 and MCF7 cells, compared to GAPDH (loading control). b The histogram presents mean values (± SEM) of the ratio ANX/GAPDH from five independent experiments, analyzed by the gel analysis plugging of ImageJ. A representative membrane of the detection of ANXA1 is presented in supplementary Figure 1. Student t-test for independent samples. **: $p < 0.01$.

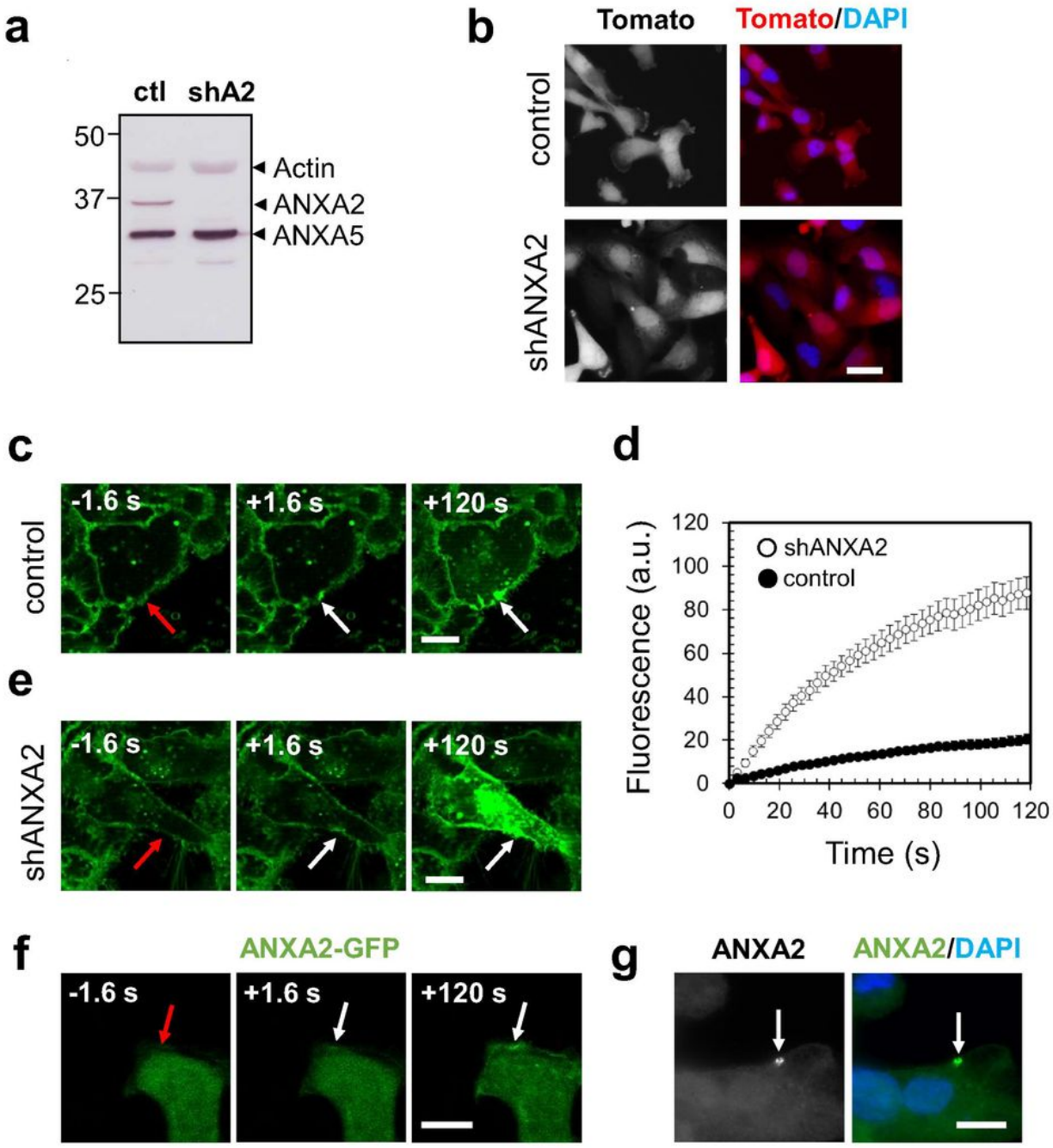

Figure 2

ANXA2 is required for membrane repair in MDA-MB-231 cells. a ANXA2 deficient MDA-MB-231 cells was generated by shRNA transduction strategy. The cellular content of ANXA2 in MDA-MB-231 cells transduced with lentiviral particles containing shRNA targeting ANXA2 (shA2) or a scrambled shRNA (ctl) was quantified by Western blotting. The expression of ANXA2 is decreased of more than 90% in shANXA2 MDA-MB-231 cells. b Control and shANXA2 MDA-MB-231 cells, which expressed constitutively the

tdTomato fluorescent protein were imaged by fluorescence microscopy. c, e Sequences of representative images showing the response of a control (c) or shANXA2 (e) MDA-MB-231 cell to a membrane damage performed by 110-mW infrared laser irradiation, in the presence of FM1-43 (green). In all figures, the area of membrane irradiation is marked with a red arrow before irradiation and a white arrow after irradiation. Scale bars: 10 μm. d Kinetic data represent the FM1−43 fluorescence intensity integrated over whole cell sections, averaged for about 30 cells (+/−SEM). For a majority of control MDA-MB-231 cells, the fluorescence intensity reached a plateau after about 80 s (black filled circles). For shANXA2 MDA-MB-231 cells, a continuous and large increase of the fluorescence intensity was observed (empty circles), indicating the absence of membrane resealing. f Recruitment of ANXA2 to the site of membrane injury. MDA-MB-231 cells transfected with the plasmid pA2-GFP were damaged by laser ablation. Red arrow, area before irradiation; white arrow, area after irradiation. g Subcellular localization of endogenous ANXA2 in damaged MDA-MB-231. MDA-MB-231 cells were irradiated with a 110-mW infrared laser (white arrow) in DPBS + Ca2+, then fixed and immunostained for ANXA2 and counterstained with DAPI (blue). After laser injury, MDA-MB-231 cells exhibited an accumulation of ANXA2 at the disruption site. Scale bars: 10 μm.

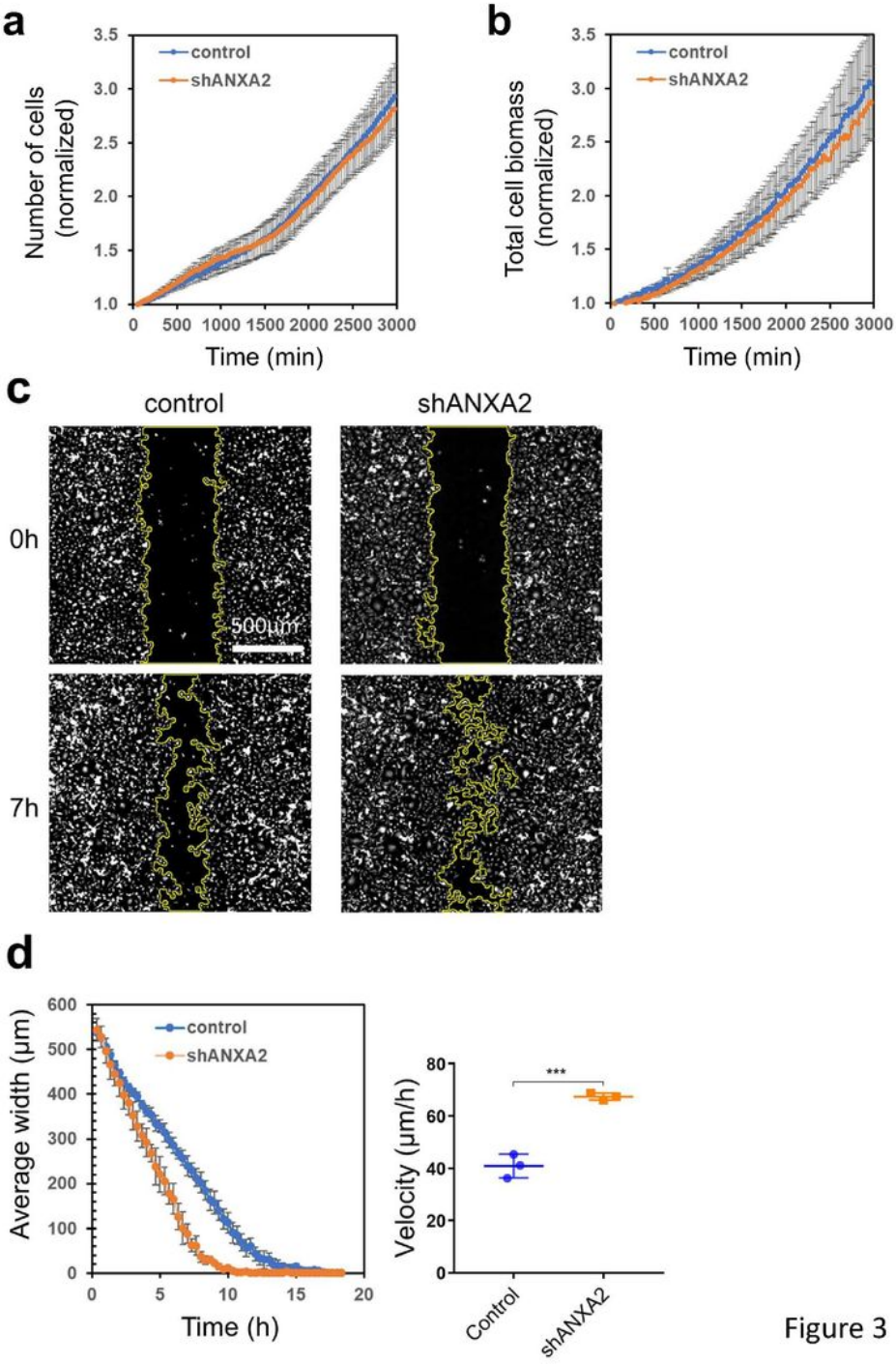

Figure 3

Figure 3

Proliferation and 2D-migration of MDA-MB-231 cells are independent from ANXA2. a-b Proliferation of control or shANXA2 MDA-MB-231 cells was monitored with a lensfree microscope enabling continue observation of a large cell population40. One image was acquired every 25 min. Phase images were analyzed using Trackmates2 on Fiji and MATLAB. a Averaged number of cells (+/- SEM) normalized to the number of seeded cells from three independent experiments. b Normalized total cell biomass (+/-

SEM), which considers individual number and cell size, from three independent experiments. c-d In vitro 2D-migration assay was performed on control or shANXA2 MDA-MB-231 cells. 3.5 x 105 cells/well were plated into culture-Insert 2-well in 35 mm µ-Dish (Ibidi) coated with 0.5 mg/mL gelatin. Cell progression was monitored with a lensfree microscope40, after removing the culture insert. c Typical images of control or shANXA2 MDA-MB-231 cells immediately or 7h after insert release are presented. Migration front is drawn in yellow. d Mean gap closure kinetics and cell velocity measure (+/- SEM) from three independent experiments are presented for each cell type. Non-parametric Mann-Whitney test. ***: $p < 0.001$.

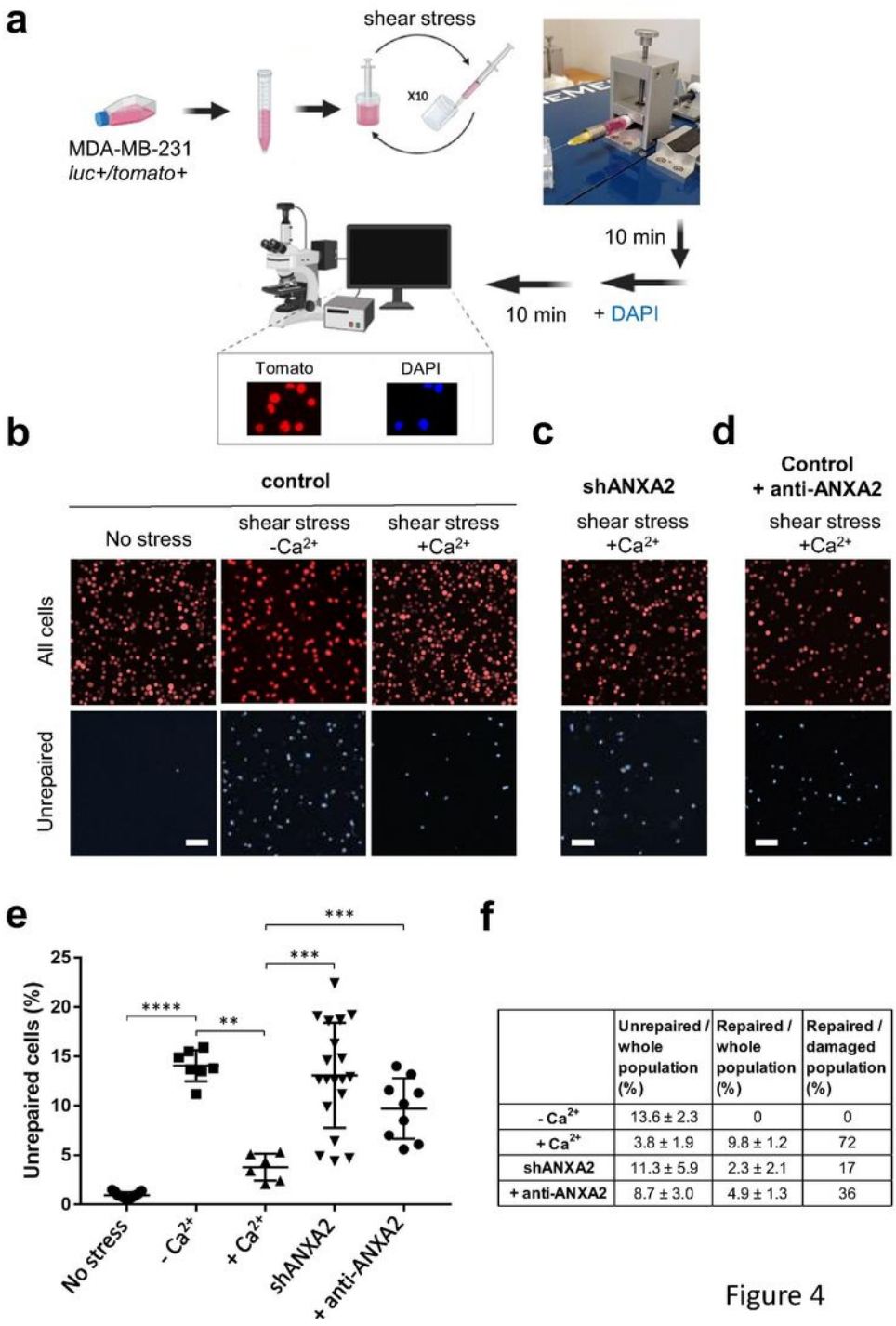

	Unrepaired / whole population (%)	Repaired / whole population (%)	Repaired / damaged population (%)
- Ca^{2+}	13.6 ± 2.3	0	0
+ Ca^{2+}	3.8 ± 1.9	9.8 ± 1.2	72
shANXA2	11.3 ± 5.9	2.3 ± 2.1	17
+ anti-ANXA2	8.7 ± 3.0	4.9 ± 1.3	36

Figure 4

Figure 4

Response of control or shANXA2 MDA-MB-231 cells to membrane injury by shear-stress treatment. a Scheme of the protocol with a photography of the device used for the automatized shear-stress treatment. The microfluidic approach is based on a method initially devoted to introduce large macromolecules into mammalian cells41. 5 x 105 cells/mL cells were loaded in a 1 mL syringe with a 30G needle mounted on a fully automated NeMESYS syringe pump system (Cetoni GmbH, Korbussen,

Germany). After 10 passages through the needle, cells were incubated with DAPI, which stained damaged/unrepaired cells, while all cells expressed the fluorescent protein tdTomato. Created using Biorender.com. b Representative images of control unstressed MDA-MB-231 (left-hand panels), and stressed cells in the absence (middle panels) or presence (right-hand panels) of 2 mM Ca2+. Scale bar: 50 μm for all images. c Representative images of shANXA2 MDA-MB-231 submitted to the shear stress assay in the presence of 2 mM Ca2+. Scale bar: 50 μm. d Representative images of control MDA-MB-231 submitted to shear stress assay in the presence of 2 mM Ca2+ and monoclonal anti-ANXA2 antibody (1:50, Sigma-Aldrich). Scale bar: 50 μm. e Unrepaired cells, which are defined as DAPI-positive cells over the whole cell population (tdTomato-positive), were quantified for at least 6 independent experiments. Experimental data together with mean (+/- SEM) are presented. Non-parametric Mann-Whitney test. ** P value (<0.01), *** P value (<0.001), **** P value (<0.0001). f Mean percentage of unrepaired cells represented in e are indicated in the second column. Mean percentage

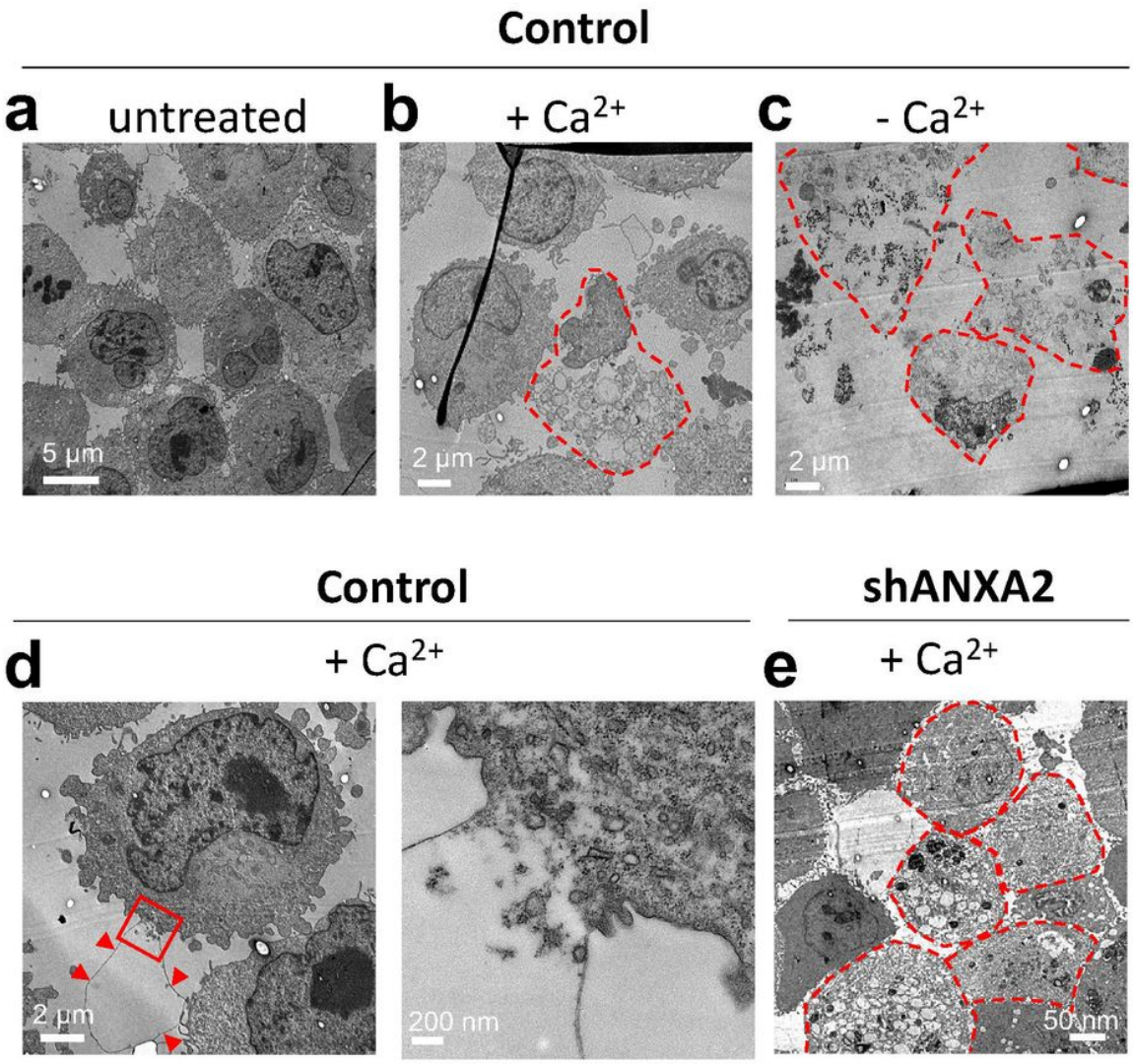

Figure 5

control and shANXA2 MDA-MB-231 cells submitted to the shear-stress treatment analyzed by TEM. Control cells submitted (b-d) or not (a) to the shear-stress treatment were fixed and embedded in Epon-Araldite. Ultra-thin sections were stained and imaged by TEM. Shear-stress treatment was performed with (b, d and e) or without (c) 2 mM Ca2+. a In the absence of treatment, the cells appear with an electron-dense cytoplasmic content and a conspicuous cell membrane. b The shear-stress treatment led frequently to the observation of cells stripped of their content (red dotted line). c In the absence of Ca2+, this effect was accentuated (cells with red dotted line). d In the presence of Ca2+, many cells exhibited isolated micrometric membrane damage (red square), which seemed to be resealed. The right-hand image displays a high-magnification of the area present within the red square. Red arrowheads point out

the large bleb protruded from the site of damage. e Most shANXA2 MDA-MB-231 cells submitted to the shear-stress treatment appeared to have lysed (red dotted line) in the presence of Ca2+.

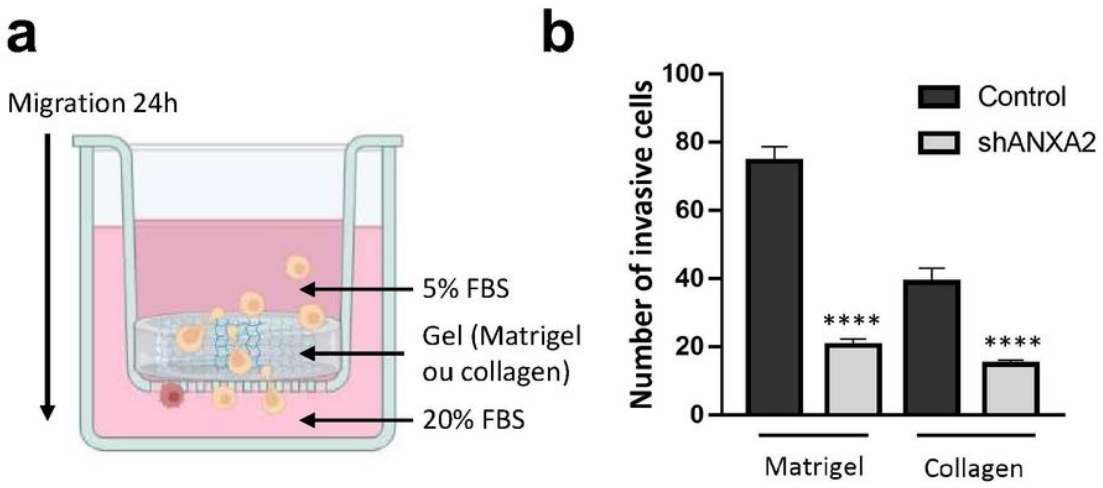

Figure 6

Figure 6

ANXA2 deficiency impairs MDA-MB-231 cell invasion. a A Matrigel or dense collagen gel was produced into a transwell and cells were seeded in media with 5% FBS on top of the gel. As chemoattractant, 20% FBS-containing medium was added in the bottom of the well to allow cell invasion through the gel. Created using Biorender.com. b Number of control or shANXA2 MDA-MB-231 cells able to cross the gel was quantified. Unpaired Student t-test. ****: $p < 0.0001$.

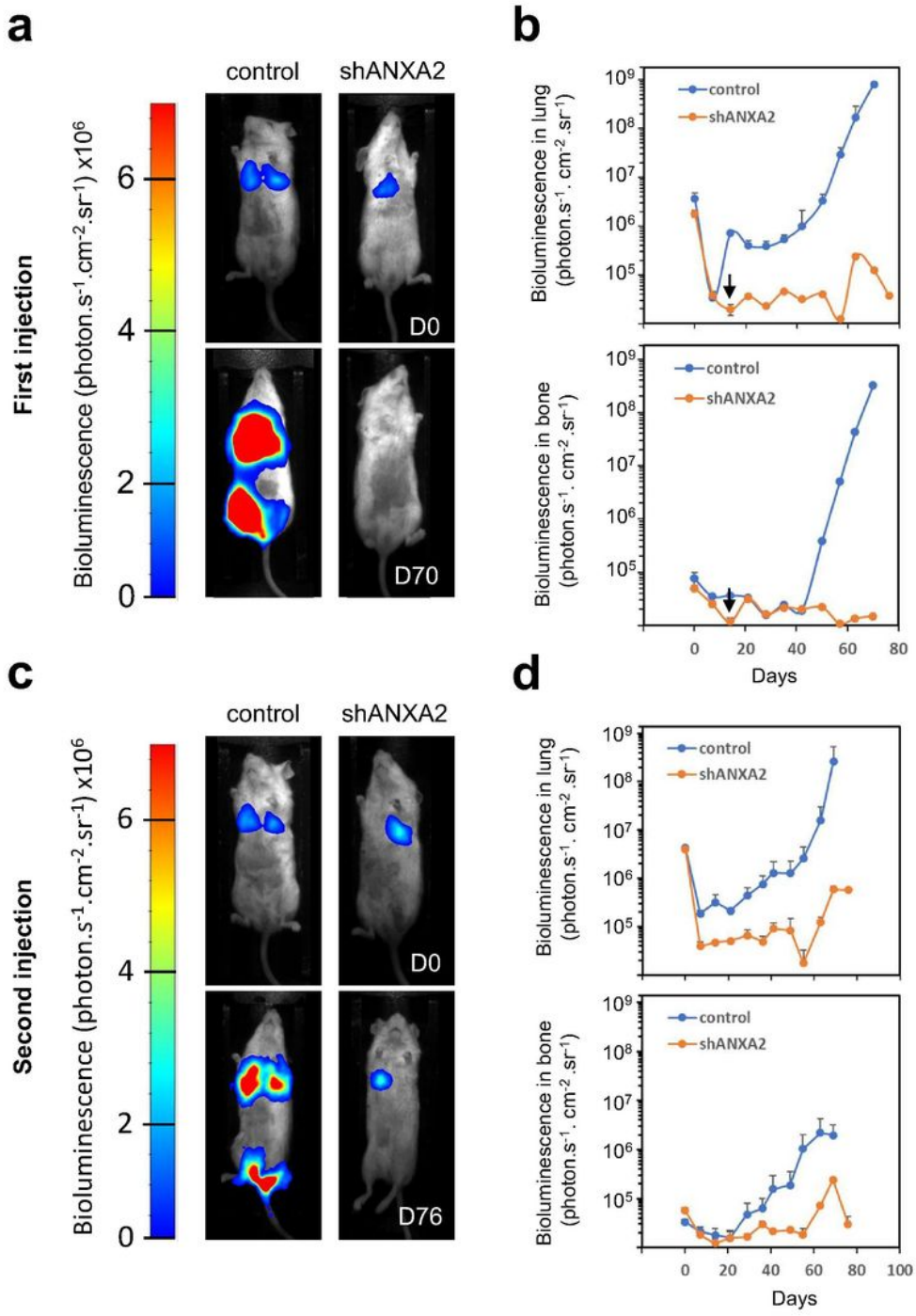

Figure 7

Genetic inhibition of ANXA2 prevents tissue colonization of MDA-MB-231 cells in NOD SCID mice. a Control or shANXA2 MDA-MB-231 cells were injected in NOD SCID mice as described in the legend of the Supplementary Figure 5. Representative bioluminescence images of NOD SCID mice 30 min (D0) or 70 days (D70) after injection of MDA-MB-231 cells are presented. b Bioluminescence quantification in lungs and bone for control (n =5)

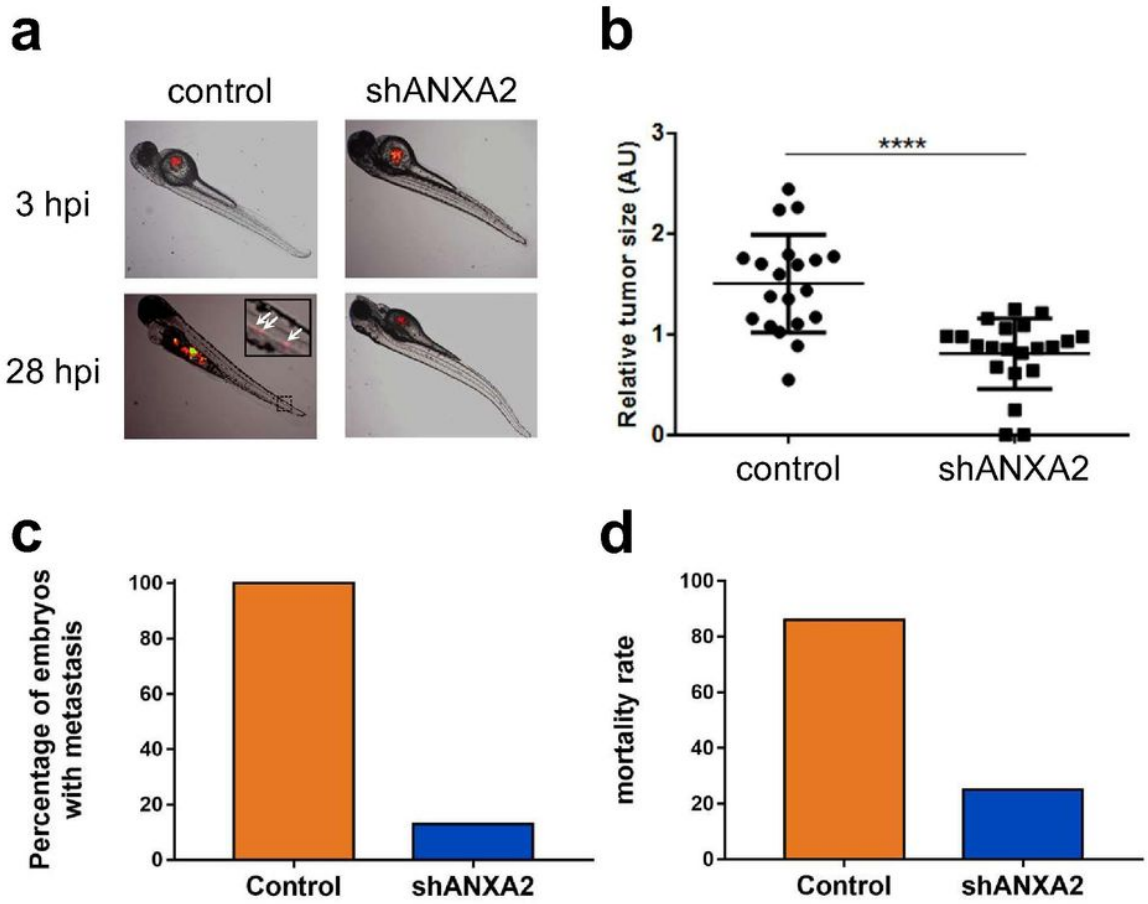

Figure 8

Figure 8

Genetic inhibition of ANXA2 prevents invasion and metastasis processes of MDA-MB-231 cells in zebrafish. a Control (n = 21) or shANXA2 MDA-MB-231 (n = 24) cells were injected in the perivitelline space of Casper zebrafish embryos. Tumor imaging was done by fluorescence microscopy at 3-, 28- and 52 hpi through the tdTomato fluorescent protein constitutively expressed in MDA-MB-231 cells. Inset displays magnified image of a portion of the tail with metastases (white arrows). b The relative tumor size within the perivitelline space has been measured in embryos either injected by control or shANXA2 cells. c The percentage of embryos, which presented caudal or head metastases was quantified at 28 hpi. d Mortality rate was calculated at 52 hpi.

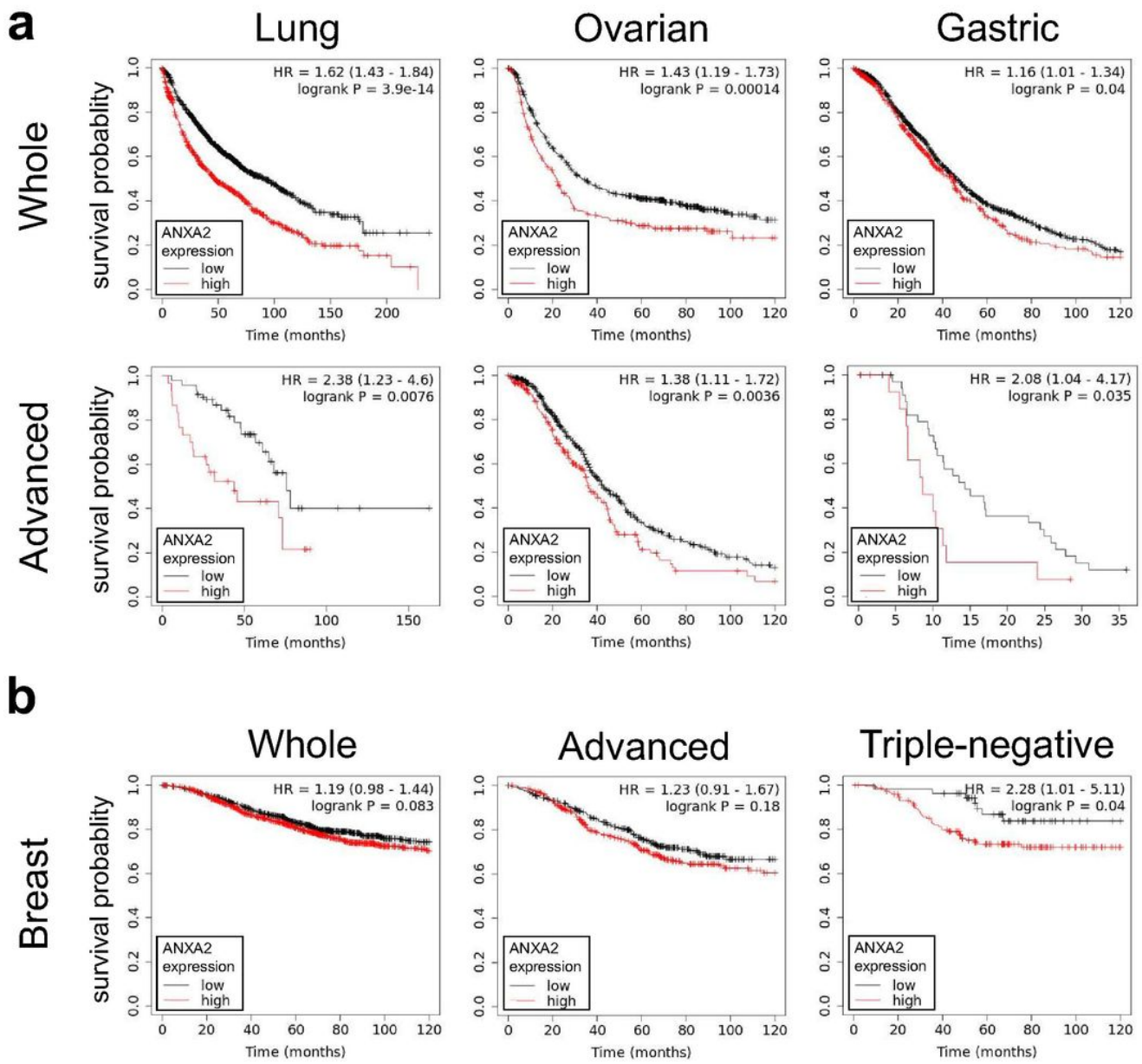

Figure 9

High ANXA2 expression in cancer patients is a factor of poor prognosis. Survival curves from Kaplan-Meier plot profiles39 for lung, gastric, ovarian and breast cancer patients stratified by high and low expression of ANXA2 mRNA (Affymetrix identifier, 201590_x_at). Analysis was performed either over the whole patient population or patients suffering from advanced cancer, characterized by high grade and/or stage. To note, cancer grade (typically numbered from 1 to 3) correlates with the velocity of the disease development while stage (from 1 to 4) characterizes the extent of affected tissues. High-grade and -stage cancers are often very aggressive, with strong tumor invasion and the presence of metastatic cells, respectively. In each analysis, hazard ratio (HR) and log-rank probability were calculated. A HR

significantly different from 1 means that survival was better in one of both groups. For example, if a HR is 1.5, the survival probability in group 1 is 1.5 higher than in group 2. a Survival curves for lung (n = 1925), ovarian (n = 1656) or gastric (n = 875) cancers within the whole patient population (whole, first row) or patients suffering from advanced cancer (advanced, second row). Advanced cancers were grade 3, stage 3 + grade 3, and stage N > 1 + M = 1, for lung (n = 77), ovarian (n = 744) and gastric (n = 51) cancer, respectively. b Survival curves for the whole breast cancer patients (n = 1879) or those with an advanced disease (stage N = 3; n = 586). Triple-negative is an invasive and aggressive form of breast cancer that is estrogen receptor-negative, progesterone receptor-negative, and HER2-negative.

Supplementary Files

This is a list of supplementary files associated with this preprint. Click to download.

- MsCancerRepairANXA2BouterSUPPINFO.pdf